Spin-Forbidden Ligand Binding to the Ferrous−Heme Group: Ab Initio and DFT Studies

Nikki Strickland and Jeremy N. Harvey*

Centre for Computational Chemistry and School of Chemistry, University of Bristol, Cantock's Close, Bristol, BS8 1TS, United Kingdom

Received: June 29, 2006; In Final Form: November 18, 2006

The potential energy surfaces (PESs) and associated energy barriers that characterize the spin-forbidden recombination reactions of the gas-phase ferrous deoxy−heme group with CO, NO, and H_2O ligands have been calculated using density functional theory (DFT). The bond energy for binding of O_2 has also been calculated. Extensive large basis set CCSD(T) calculations on two small models of the heme group have been used to calibrate the accuracy of different DFT functionals for treating these systems. Pure functionals are shown to overestimate the stability of the low-spin forms of the deoxy−heme model, and to overestimate the binding energy of H_2O and CO, whereas hybrid functionals such as B3PW91 and B3LYP yield accurate results. Accordingly, the latter functionals have been used to explore the PESs for binding. CO binding is found to involve a significant barrier of ca. 3 kcal mol^{-1} due to the need to change from the deoxy−heme quintet ground state to the bound singlet state. Binding of water does not involve a barrier, but the resulting bond is weak and may be further weakened in the protein environment, which should explain why water binding is not usually observed in heme proteins such as myoglobin. NO binding involves a low barrier, which is consistent with observed rapid geminate recombination. The calculated bond energies are in good agreement with previous reported values and in fair agreement with experiment for CO and O_2. The value for NO is significantly lower than the experimentally derived bond energy, suggesting that B3LYP is less accurate in this case.

Introduction

The binding and dissociation reactions of small ligands such as O_2, CO, and NO with heme proteins are important biological processes. Transport and storage of dioxygen is possible in living organisms because of the reversible reaction of O_2 with hemoglobin and myoglobin, respectively. The interaction of NO with heme proteins has been linked to a number of biological functions,[1] including the inhibition of mitochondrial respiration[2] and neurotransmission.[3] The most widely studied heme protein is myoglobin, which is composed of 153 amino acid residues, eight α-helices, and a ferrous−heme cofactor. The latter interacts with the polypeptide chain through a covalent Fe−N bond to the $N_{\epsilon 2}$ of histidine 93 (the proximal histidine) and hydrogen bonds to the heme propionate side chains. In the absence of further ligands, the iron atom is penta-coordinate. This form of the protein is referred to as deoxy−myoglobin. Small ligands that reach the distal cavity above the porphyrin plane can bind reversibly at the sixth coordination site, forming, for example, oxy−, carbonmonoxy−, or nitroxy−myoglobin. The iron atom can also be oxidized to an inactive ferric (III) oxidation level, where it can bind to a water molecule, yielding aquomet− (or met) myoglobin.

We wish to understand the mechanism of the ligand binding step, once the ligand has moved from the solvent through the protein and reached the distal cavity. This binding step has been extensively studied after flash photolysis of the CO, O_2, or NO ligand[4−9] and involves a small energy barrier, known as the recombination barrier, which varies between ligands.[10] At lower temperatures, diffusion out of the distal pocket is inhibited, and

recombination can be studied in great detail. This has led to the identification of interesting kinetic features such as ligand tunneling[11] and non-homogeneous decay due to the presence of multiple protein substates. These substates interconvert on a slower time scale than that for recombination[4] and have different intrinsic addition barriers to ligand binding.

H_2O does not usually add to the heme group of ferrous deoxy−myoglobin, even at low temperature where entropic effects are small, despite being able to reach the distal cavity. This suggests that bonding is either impeded by a large barrier or is not enthalpically favorable under normal conditions. Under certain conditions, however, water binding is thermochemically and kinetically feasible. Metastable ferrous aquo−myoglobin has been observed following low-temperature reduction of ferric metaquo−myoglobin.[12] This ferrous aquo−myoglobin complex is stable at temperatures below 150 K and exhibits a similar geometry to that of ferric aquo−myoglobin. Like O_2, NO, and CO, water can even be photodissociated from the heme iron under these conditions, followed by spontaneous rebinding.[13] This shows that for this form of myoglobin at least, water binding is thermodynamically favorable. The authors speculate that the absence of such a reaction in relaxed deoxy−myoglobin is because the heme iron is too far out of the heme plane to form a sufficiently strong bond with the water ligand.

Recombination of NO after photodissociation has been studied extensively[5,6,8] and occurs on a faster time scale than CO and O_2 binding.[10] One suggested reason for this is the so-called harpoon mechanism,[14] whereby fast rebinding occurs because the unpaired NO electron and the electron in the Fe d_{z^2} orbital form a bond without the heme iron having to move into the porphyrin plane. The suggestion is that this mechanism cannot occur in the case of CO and O_2 binding, which instead requires

* Corresponding author. E-mail: Jeremy.harvey@bristol.ac.uk. Fax: +44 (0)117 925 1295. Tel.: +44 (0)117 954 6991.

energetically costly concerted motion of the protein and heme group before the reaction can occur. An alternative report suggests that the reaction occurs via a metastable MbON intermediate that subsequently isomerizes to MbNO.[15]

For the reactions of small ligands, such as O_2, CO, NO, and H_2O, with ferrous deoxy−myoglobin, the need to change the spin-state may contribute to the intrinsic additional barrier.[16,17] Ferrous deoxy−myoglobin has a high-spin quintet iron atom, while oxy− and carbonmonoxy−myoglobin have singlet ground states, and nitroxy−myoglobin is a doublet. This means that the so-called spin-forbidden reactions of singlet CO, doublet NO, or triplet O_2 with the heme group require at least one spin-state change. During a spin-state change, the system crosses from the potential energy surface (PES) corresponding to one spin-state to that of a different spin-state. Such spin-forbidden reactions are common in transition metal chemistry,[18,19] and hence bioinorganic chemistry, because changes in the ligand field around the metal center during reaction can lead to ground states with different multiplicity for reactants and products. If there is strong spin−orbit coupling between the two wavefunctions corresponding to each PES, as is often the case in transition metal chemistry, the strong avoidance of the crossing region will probably mean that the process is forbidden by only a small degree. However, the topology of the individual surfaces and of their avoided crossing may lead to a significant barrier to reaction.

We have shown before that reactivity in spin-forbidden reactions can be rationalized by locating the minimum energy crossing points (MECPs) between the potential energy surfaces corresponding to the different spin-states involved.[19−23] The relative energy and other properties of these points can yield qualitative and indeed quantitative predictions of reactivity. Notably, we have shown that some spin-forbidden reactions are extremely fast due to a favorable topology of the surface crossing, while others can be slowed by the need to undergo a spin-flip.[21,23]

There is considerable previous computational work in the literature on the binding of small ligands to the heme group.[24−39] Many of these use DFT methods, and by and large, results obtained using similar functionals by different groups are similar to one another, so we will focus our discussion on only a few of these papers. We also note that the list of papers cited previously is not exhaustive. Rovira et al. studied binding of CO, NO, and O_2 to an iron−porphine−imidazole model using the BP86 density functional method.[28] They obtained geometries in good agreement with experiment and binding enthalpies of, respectively, 15, 35, and 36 kcal mol^{-1} for O_2, CO, and NO. Using an iron porphine−ammonia model of the heme group together with the B3LYP method, Blomberg et al. reported binding energies of 7.6, 12.5, and 16.9 kcal mol^{-1} for O_2, NO, and CO.[38] Some of these studies also attempt to model the way in which the environment of the heme group in proteins such as myoglobin modulates the binding energy of the different ligands by including some surrounding residues in the QM model system[25,27,29,38] or by using a QM/MM treatment of the whole protein.[32,39] Some of the previously mentioned computational studies by other groups[31,33,34,36] have also explored the regions in which the PESs of the different spin-states cross each other as the ligand approaches the metal. In these studies, the MECPs between the relevant potential energy surfaces have been located in an approximate way, usually by fixing most of the coordinates at their equilibrium values for the bound or deoxy state and mapping out the potential energy surfaces along a small number of few key coordinates such as the Fe−X

distance.[31,33,34] In another case, approximate MECPs have been located using the partial optimization method,[20] in which one degree of freedom is systematically varied and the rest of the geometry optimized at fixed values of this coordinate.[36]

In our own work, we have explored the binding of CO to a model of the heme group and found a MECP lying 2.4 kcal mol^{-1} above the deoxy−heme reactant.[30] Using the properties of the MECP, and a non-adiabatic form of transition state theory, the rate coefficient for recombination was computed to be in reasonable agreement with the experimental value, given that the protein environment of Mb is expected to influence the reaction.[40] The NA-TST calculations also show that CO recombination is highly non-adiabatic, occurring roughly 300 times slower than would be the case for an analogous spin-allowed barrier crossing. We have also reported hybrid QM/MM studies of the singlet and quintet potential energy surfaces in the solvated real protein system.[40] and a detailed study of how the environment of myoglobin influences the Fe−CO bond energy.[39] In such work, the core porphyrin and CO atoms are described using quantum mechanical (QM) density functional theory (DFT), while the bulk atoms are treated with molecular mechanics (MM). Our ongoing work on surface crossings in myoglobin is beginning to give an atomistic insight into the way in which the protein environment affects reactivity in these important heme systems.

We hereby extend our study to the intrinsic properties for binding of CO, NO, H_2O, and O_2 to the ferrous deoxy−heme group, including a description of the MECPs involved in spin-state changes for binding of CO, NO, and H_2O. As part of this work, we first examine the accuracy of DFT for treating heme systems. Much of our previous work, including the study of CO binding to ferrous deoxy−heme,[30] has used the popular hybrid B3LYP density functional[41] due to its overall high accuracy for main-group systems[42] and good performance for many bioinorganic systems.[43,44] However, it is well-known that the different DFT functionals can yield very different relative spin-state energetics,[35,45] and we have, in particular, found that pure functionals such as BP86[46,47] can yield better spin-state energetics than B3LYP for some transition metal systems.[23] There is limited experimental evidence available to calibrate how well DFT treats heme compounds, although some crystal structures exist with which to calibrate the geometry predictions. We have therefore carried out high-level CCSD(T) calculations with large basis sets on porphyrin model systems and have calibrated our DFT relative spin-state energies and bond dissociation energies (BDEs) against these CCSD(T) values. For the BDE calibration, we focus on the energies of the Fe−CO and Fe−OH$_2$ bonds because equivalent calculations on the Fe−NO and Fe−O$_2$ bonds are currently beyond our computational resources due to the complex electronic structure of these adducts.

Our calculations use three molecular systems, shown in Figure 1, to represent the heme group. The largest and most realistic is FeP(Im), where P is a porphine ring and Im is an imidazole group. FeP(Im) has been used to investigate the reactions of CO, NO, O_2, and H_2O with deoxy−heme and to assess how well DFT predicts heme-type geometries. The smaller models **1** and **2** are [Fe(C$_n$H$_{n+2}$N$_2$)$_2$(OH$_2$)], where $n = 1$ or 3, respectively. Models **1** and **2** are necessary for the calibration studies because FeP(Im) is too large to be treated with CCSD-(T), although some calibration work has been carried out on iron−porphine systems using CASSCF and CASPT2 multi-reference methods.[48] Small models similar to **1** and **2** have been shown previously to reproduce some of the features of the larger
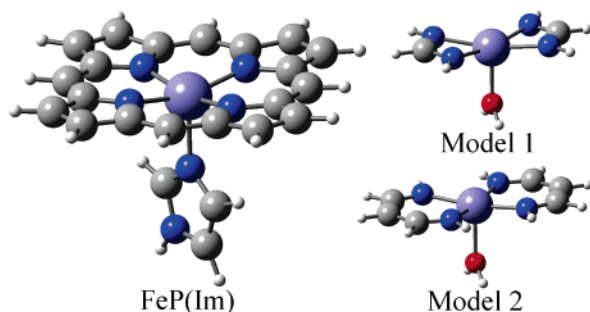
Figure 1. Molecular structures of FeP(Im), model **1** [Fe(CH$_3$N$_2$)$_2$-(OH$_2$)], and model **2** [Fe(C$_3$H$_5$N$_2$)$_2$(OH$_2$)].

model.[27,43,49] Our larger model **2** is more similar to the FeP-(Im) system; hence, the accuracy of DFT in treating this model is likely to be the best reflection of how different functionals predict the energies of iron−porphyrin systems. The smaller size of model **1** allows CCSD(T) computations with a slightly larger basis set and so provides a useful indication of whether to expect any basis set dependence in our model **2** calculations. In the models, the combination of the two amidine CH$_3$N$_2^-$ or vinylogous amidine C$_3$H$_5$N$_2^-$ ligands has the same charge and bonding geometry as the full porphyrin ring. Neither model is cyclic; hence, they differ from the FeP(Im) system in their conjugation properties. In this respect, model **2** is more similar to FeP(Im) than model **1**, with the same number of sp^2 carbon atoms between the nitrogens as in the porphyrin of FeP(Im) and so a more similar bite angle. The water molecule in both models was chosen to represent the imidazole ligand because of its small size, high symmetry, and donation of a single lone pair to the metal center.

Computational Details

DFT geometry optimizations of models **1** and **2** and the FeP-(Im) systems were carried out with the Jaguar electronic structure package,[50] using the standard gradient corrected BP86[47] and BLYP[51] functionals and the hybrid B3LYP,[41] B3PW91,[52] and B3P86 functionals.[53] A restricted or restricted open-shell formalism was used throughout except where mentioned otherwise. For the bound form of O$_2$, which is an open-shell singlet, an unrestricted formalism was used, and for consistency, UDFT calculations were then carried out on the corresponding fragments. Except for the bound O$_2$, modest spin-contamination was observed in all cases when using UDFT (e.g., the expectation value of the S^2 operator is ca. 6.04 for quintet FeP(Im) vs 6.00 for a pure quintet). The standard Los Alamos ECP with the Jaguar triple-ζ basis (LACV3P) was used for Fe, and the 6-311G* basis was used for all other atoms, including the H$_2$O, CO, O$_2$, and NO ligands. The optimum geometries for the models **1** and **2** display various distortions from the idealized symmetric structures shown in Figure 1, such as pyramidalization at nitrogen or rotation of the water molecule. These distortions decrease the similarity with the full porphyrin system and lower the symmetry, thus making the CCSD(T) computations intractable. To avoid this, all systems were constrained to have either C$_{2v}$ (deoxy and carbonmonoxy models) or D$_{2h}$ (aquo model) symmetry, and all atoms in the nitrogen-containing ligands (not including the iron) were constrained to lie in a single plane. All calculations were carried out using ultrafine DFT and pseudo-spectral grids.

The single-point CCSD and CCSD(T) energies were computed for models **1** and **2** at the previous B3LYP geometries, using the MOLPRO program package.[54] The cc-pVXZ (X =

D, T, or Q) correlation consistent basis sets of Dunning et al.[55] were used on carbon, oxygen, nitrogen, and hydrogen. Iron was treated with the cc-pVTZ or cc-pVQZ basis sets of Ricca and Bauschlicher.[56] For extrapolation to the infinite basis limit, one would normally use the same basis (e.g., cc-pVTZ or cc-pVQZ) on all atoms of the molecule, but this was not computationally feasible. Instead, we have divided the molecules into two parts, which are treated using differently sized basis sets: the iron atom and its sixth ligand, if present, form one part, with the spectator amidine and water ligands forming the other. The iron atom and ligand have been treated using the larger cc-pVTZ and cc-pVQZ bases, whereas the amidine and water ligands could only be treated with cc-pVDZ or, for model **1**, cc-pVTZ. Additionally, all hydrogen atoms in all calculations were treated with the cc-pVDZ basis. Assuming that the correlation energy on the two parts is roughly additive, and that the computed spin-state splitting and bond energies are not heavily dependent on the basis of the amidine ligand, it is then possible to extrapolate to the infinite basis limit using the results obtained with the cc-pVTZ and cc-pVQZ bases on iron (and its ligand) and the 1/X^3 dependence of the residual correlation energy on the basis set size proposed by Helgaker et al.[57]

We note that the additivity assumption for the correlation energy is not likely to be exact, as some electron pairs are shared between iron and the amidine ligands. The extrapolated results using cc-pVDZ and cc-pVTZ on the amidine ligands are slightly different, showing that the correlation effects cannot be rigorously separated. Another potential problem with our approach is that it is not clear how to apply the 1/X^3 law, as the maximum angular momentum basis functions present in the cc-pVXZ bases for iron do not match those for C, N, and O: cc-pVTZ has g functions ($l = 4$) on iron, and cc-pVQZ has h functions. We nevertheless use $X = 3$ for cc-pVTZ and $X = 4$ for cc-pVQZ in our extrapolation but recognize that this will not reproduce the exact basis set dependency. The difference in the computed values obtained by extrapolating using $X = 4$ and 5 instead is, however, smaller than the other uncertainties affecting our results. Hence, $E_\infty = E_{HF-cc-pVQZ} + 64/37E_{correl/cc-pVQZ} - 27/37E_{correl/cc-pVTZ}$, with the basis held constant at either cc-pVDZ or cc-pVTZ on the amidine ligands.

The counterpoise corrections for basis set superposition errors (BSSE) were included for each calculated CCSD(T) BDE. This correction was based on the energy difference between calculations on the fragments at the geometry of the whole complex using the fragment basis sets only and the full basis set of the whole complex.

For the larger FeP(Im), the variation of energies with functionals were established using full geometry optimizations without constraints, ultrafine DFT, and pseudo-spectral grids for the standard gradient corrected BP86 and BLYP functionals and the hybrid B3LYP, B3P86, and B3PW91 functionals. The basis sets used were the standard Los Alamos ECP with the Jaguar triple-ζ basis (LACV3P) for Fe, the standard 6-311G* basis for all nitrogen atoms and the CO, NO, O$_2$, and H$_2$O ligands, and the 6-31G* basis (with five spherical harmonic d polarization functions) on carbon and hydrogen. Because of the high computational cost of calculating vibrational frequencies for the large FeP(Im) systems, and the difficulties in calculating frequencies for MECPs, none of the calculated energetics includes a correction for zero-point energy.

The geometry and energy of the crossing points between unligated high-spin potential energy surfaces and ligated low-spin surfaces were determined by optimizing the geometry of the corresponding minimum energy crossing points (MECPs).

TABLE 1: DFT Energies[a] of Triplet and Singlet States of Model Heme Compounds

	FeP(Im)		model **1**		model **2**	
functional	^{3}[Fe]	^{1}[Fe]	^{3}[Fe]	^{1}[Fe]	^{3}[Fe]	^{1}[Fe]
BP86	−10.5	−12.6	0.9	23.6	−20.5	2.8
BLYP	−10.6	−11.7	1.1	21.2	−17.9	3.3
B3PW91	2.8	9.6	13.6	37.8	−4.2	20.8
B3P86	0.2	5.0	10.9	33.7	−7.3	16.2
B3LYP	−0.2	5.1	10.7	31.3	−5.6	16.1

[a] In kcal mol^{-1}, relative to the quintet state.

These calculations used the method previously described,[58] where the Jaguar program was used to calculate the energy and gradient on the two surfaces. A Fortran program was then used to calculate the effective gradient pointing toward the MECP and to update the geometry. Input and output from Jaguar and the Fortran code were driven using a set of shell scripts. These MECP calculations were carried out without constraints, using ultrafine DFT and pseudo-spectral grids with the same functional and basis set choice as for the reactant and product geometry optimizations. To identify the energy minima connected by a given MECP, full geometry optimizations were carried out on each surface starting at the MECP.

Results and Discussion

(1) DFT Calibration. We start by assessing the behavior of the different functionals by comparing the DFT energies with the CCSD(T) calculated values, beginning with the relative energies of the different spin-states of the deoxy form of the three models. The DFT results are summarized in Table 1. It can be noted that the pure functionals predict much lower relative energies than the hybrid functionals for the intermediate- and low-spin triplet and singlet states as compared to the quintet reference state. This is a common observation for transition metal compounds.[45] It is usually explained by noting that the Hartree−Fock method, which includes an exact treatment of electron exchange, artificially favors high-spin states because it does not describe the correlation of electrons of opposite spin. Including a proportion (20% for the functionals used here) of Hartree−Fock exchange in hybrid functionals also favors high-spin states.

High-spin states are significantly more favored in model **1** than for the full porphyrin case, with the hybrid functionals predicting the singlet and triplet to lie more than 30 kcal mol^{-1} above the quintet ground state for model **1**. The energetics of model **2** are closer to those of the larger system, with hybrid functionals predicting closer lying quintet and triplet states and less unstable singlets. This may be because the larger bite angle of the bigger amidine ligands better reproduces the ligand field of the porphyrin ring.

We now examine how well the DFT results in Table 1 for models **1** and **2** compare to the relevant CCSD(T) results in Table 2. Before comparing the data in detail, it is worth stressing that the accuracy of our CCSD(T) calculations is unknown. Similar calculations on main-group compounds with well-defined single-reference behavior would yield energetics to within 1−2 kcal mol^{-1} or better. It is often considered that single-reference methods such as CCSD(T) are not reliable for transition metal compounds such as those studied here because correlation of compact doubly occupied metal d orbitals, and of weak metal−ligand bonding electron pairs, tends to require a multi-reference description. We note that coupled-cluster methods, especially CCSD(T) due to its inclusion of many of the effects of triple excitations, actually give rather good results

TABLE 2: CCSD(T) Energies[a] of Triplet and Singlet States of Model Heme Compounds

basis set		model **1**		model **2**	
Fe	amidines	^{3}[Fe]	^{1}[Fe]	^{3}[Fe]	^{1}[Fe]
cc-pVTZ	cc-pVDZ	20.7	42.7	3.7	25.9
cc-pVTZ	cc-pVTZ	21.7	43.4	b	b
cc-pVQZ	cc-pVDZ	18.4	39.4	0.3	22.1
cc-pVQZ	cc-pVTZ	20.2	40.9	b	b
cc-pV∞Z	cc-pVDZ	16.9	37.3	−2.0	19.6
cc-pV∞Z	cc-pVTZ	19.1	39.3	b	b

[a] In kcal mol^{-1}, relative to the quintet state. [b] Calculations too large to be feasible.

even in borderline multi-reference systems.[59] Also, one traditional measure of multi-reference character, the t_1 diagnostic,[60] suggests that the species here do not have a particularly high level of multi-reference character—the t_1 diagnostic lies between 0.007 and 0.037, well within the range for which CCSD(T) gives reliable results for main group compounds.

It should also be noted that there is no reason why a single functional could be expected to give good results for all observables for all the species considered. Hence, even if one functional predicts the spin-state splitting for model **1** correctly, as judged by comparison to CCSD(T), it will not necessarily give accurate bond energies for FeP(Im) or myoglobin. Any system dependence is more likely to occur when the electronic structure of the systems under consideration is more different. In this regard, model **2**, which yields energies closer to those obtained for FeP(Im), and is also more similar in structural terms, is perhaps a better reference for calibration than model **1**.

These provisos aside, it can first of all be seen in Table 2 that the large basis sets used here are close to convergence with respect to the computed spin-state splittings. Upon increasing the basis on iron from cc-pVTZ to cc-pVQZ or on the amidine ligands from cc-pVDZ to cc-pVTZ, changes in relative energetics of less than 3 kcal mol^{-1} are obtained. Even the correlation treatment is apparently fairly well-behaved, as the CCSD results (Table S1 of the Supporting Information) are also fairly close to the CCSD(T) ones (maximum difference of 10 kcal mol^{-1}). These two trends suggest that the CCSD(T) energies at the infinite basis set extrapolated limit should be fairly reliable, with errors greater than 5 kcal mol^{-1} unlikely.

Our first calibration test for DFT is the ability to predict the relative energies of different spin-states of the heme group. As expected from the FeP(Im) energies, comparing Tables 1 and 2 shows that the pure functionals cannot be relied upon to yield an accurate description of the electronic structure of heme-type compounds. The errors are significant: for both model **1** and model **2**, the pure functionals predict the triplet and singlet to be up to 20 kcal mol^{-1} more stable relative to the quintet than the CCSD(T) results suggest. All three hybrid functionals perform much better, with the B3PW91 results for model **2** particularly close to the limiting value from CCSD(T) calculations. For model **2**, B3PW91, B3LYP, and B3P86 predict the triplet energies, relative to the quintet state, to within, respectively, 2.2, 3.6, and 5.3 kcal mol^{-1} of the CCSD(T)/ cc-pV∞Z,cc-pVDZ values. The errors on the singlet relative energies are even smaller.

It should be noted that the most accurate model **2** CCSD(T) relative energies are extrapolated from energies calculated with the cc-pVDZ basis on the amidines, whereas the most accurate model **1** CCSD(T) relative energies have been extrapolated from energies calculated with the more accurate cc-pVTZ basis on the amidines. For model **1**, the relative triplet

DFT Study of Ligand Binding to Heme

J. Phys. Chem. B, Vol. 111, No. 4, 2007 **845**

and singlet energies calculated by the less accurate CCSD(T)/cc-pV∞Z, cc-pVDZ are 2.2 and 2.1 kcal mol^{-1} lower in energy, respectively, than the analogous CCSD(T)/cc-pV∞Z,cc-pVTZ values. It is reasonable to expect the CCSD(T)/cc-pV∞Z,cc-pVTZ values of model **2** to relate to the lower basis set in the same way as the model **1** values. If this was the case, the model **2** CCSD(T)/cc-pV∞Z,cc-pVTZ triplet would be 4.2 kcal mol^{-1} less stable than the quintet, and the singlet would be 17.5 kcal mol^{-1} less stable than the quintet. For either best set of energetics, the B3PW91 functional predicts the closest triplet spin-state energy to the CCSD(T) values for model **2**. Also, the singlet spin-state energy is slightly underestimated by the B3PW91 functional and slightly overestimated by the B3LYP and B3P86 functionals. Overall, the hybrid functionals all give good results.

The B3LYP and B3P86 hybrid functionals predict near identical relative spin-state energies for FeP(Im), with the singlet being 5 kcal mol^{-1} less stable than the quintet and the triplet and quintet energies being virtually degenerate. The pure functionals, on the other hand, predict singlet ground states for FeP(Im). This is not consistent with experiment and is further evidence of the unsuitability of these functionals for this system. The very slight difference between our B3LYP relative energies calculated here and in previous work[30] is due to the discovery of a slightly more stable geometry for the triplet state, as discussed below. From our calibration work, we expect the stability of the triplet state, relative to the quintet, to be predicted most accurately by the B3PW91 functional and slightly overestimated by the B3LYP and B3P86 functionals. We also expect the stability of the singlet state, relative to the quintet, to be slightly overestimated by the B3LYP and B3P86 functionals but slightly underestimated by the B3PW91 functional. This suggests that the singlet state of deoxy−FeP(Im) lies between 5.0 and 9.6 kcal mol^{-1} higher in energy than the quintet. We note that using a decreased proportion of exact exchange (e.g., 15%)[45] would give results closer to those obtained with the pure functionals and thereby noticeably further away from the CCSD-(T) results.

Overall, the accuracy of the relative energies of the different spin-states calculated by the hybrid functionals is encouraging, especially for model **2**. Furthermore, the errors decrease with the magnitude of the energy difference between the most and the least stable of the singlet/triplet/quintet spin-states. Model **2** has smaller errors than model **1**, and the spread of spin-state energies is smaller again for the FeP(Im) system. This is indicative of hybrid functionals predicting a good level of accuracy for the relative spin-states of FeP(Im). B3PW91 appears to perform slightly better than the B3LYP and B3P86 hybrid functionals.

Our second calibration test for DFT is the prediction of the energy of bonding of a sixth ligand, CO or H_2O, to the central iron of the three different deoxy systems. We consider only the singlet ground state of the bound metal−ligand systems and focus our discussion on the BDE relative to the quintet deoxy−heme ground state unless otherwise stated. The larger basis set CCSD(T) calculations are at our computational limit, as stated at the end of the Introduction; hence, equivalent calculations with the NO and O_2 ligand are not currently possible. The DFT BDEs in Table 3 show that water is bonded fairly weakly to the metal, in fact, negative BDEs are obtained at most levels of theory for the binding of water to models **1** and **2**. The extremely negative BDEs predicted for model **1** indicate that it may not be representative of FeP(Im)(OH$_2$). The chemistry of water binding to FeP(Im) will be discussed later, and we focus here mainly on the calibration of DFT using the model systems.

TABLE 3: DFT Bond Dissociation Energies^a of Aquo- and Carbonmonoxy−Heme Compounds

	^{1}[Fe]−L BDE, relative to singlet			^{1}[Fe]−L BDE, relative to quintet		
	FeP(Im)	model **1**	model **2**	FeP(Im)^b	model **1**	model **2**
	functional (L = CO)					
BP86	36.1	54.2	47.0	48.7	34.1	44.2
BLYP	29.9	45.8	39.5	41.6	27.5	36.2
B3PW91	27.6	37.6	32.9	18.0	1.6	12.2
B3P86	29.8	40.0	35.1	24.8	8.2	18.8
B3LYP	23.3	32.8	28.0	18.1	2.8	11.9
	functional (L = H_2O)					
BP86	19.3	17.0	11.5	31.9	−6.6	8.7
BLYP	17.0	16.1	10.6	28.8	−5.1	7.3
B3PW91	17.7	15.2	10.5	8.1	−22.5	−10.3
B3P86	19.7	17.2	12.3	14.7	−16.5	−3.9
B3LYP	17.7	16.3	11.3	12.7	−15.0	−4.7

^{a} BDEs in kcal mol^{-1}, relative to singlet and quintet deoxy−heme. ^{b} Experimental BDE for a related system, Mb-CO, is 10.8 kcal mol^{-1}.[61] The computed values above need to be corrected for zero-point energy (by −4.4 kcal mol^{-1}).[39] This gives zpe corrected BDEs of 13.6 and 13.7 kcal mol^{-1}, respectively, at the B3PW91 and B3LYP levels of theory.

TABLE 4: CCSD(T) Bond Dissociation Energies^a of Aquo- and Carbonmonoxy−Heme Compounds

Fe, ligand	amidines	^{1}[Fe]−L BDE, relative to ^{1}[Fe]		^{1}[Fe]−L BDE, relative to ^{5}[Fe]	
		model **1**	model **2**	model **1**	model **2**
		basis set (L = CO)			
cc-pVTZ	cc-pVDZ	30.8	29.1	−11.9	3.2
cc-pVTZ	cc-pVTZ	31.5	b	−11.8	b
cc-pVQZ	cc-pVDZ	33.0	31.1	−6.4	9.0
cc-pVQZ	cc-pVTZ	33.5	b	−7.5	b
cc-pV∞Z	cc-pVDZ	33.9	32.6	−3.4	13.0
cc-pV∞Z	cc-pVTZ	34.9	b	−4.4	b
		basis set (L = H_2O)			
cc-pVTZ	cc-pVDZ	1.44	4.44	−41.3	−21.5
cc-pVTZ	cc-pVTZ	−1.09	b	−44.5	b
cc-pVQZ	cc-pVDZ	−0.98	5.57	−40.4	−16.5
cc-pVQZ	cc-pVTZ	0.88	b	−40.1	b
cc-pV∞Z	cc-pVDZ	0.2	6.2	−37.1	−13.4
cc-pV∞Z	cc-pVTZ	2.0	b	−37.4	b

^{a} BDEs in kcal mol^{-1}, relative to singlet and quintet deoxy−heme. ^{b} Calculations too large to be feasible.

Pure functionals greatly overestimate the stability of the ligated complexes (Table 3), as compared to the CCSD(T) limit (Table 4), relative to the separate quintet deoxy fragments and ligands. As the bond energies are computed relative to quintet fragments, the large BDEs obtained with BP86 and BLYP partly reflect the fact that these functionals overestimate the energy of the quintet fragment. Tables 3 and 4 include BDEs computed relative to the singlet deoxy fragment for comparison, and these values differ less from CCSD(T). Despite this, there are still discrepancies between the BDEs calculated by the pure functionals and the CCSD(T) values, so the pure functionals will not be considered any further here.

The hybrid functionals predict much more accurate BDEs than the pure functionals. For model **2**, the B3PW91, B3LYP, and B3P86 functionals calculate the Fe−CO BDEs to within −0.8, −1.1, and +5.8 kcal mol^{-1}, respectively, as compared to the CCSD(T)/cc-pV∞Z,cc-pVDZ value. For model **1**, there is a 1.0 kcal mol^{-1} difference between the Fe−CO extrapolated BDEs calculated using the cc-pVDZ basis on the amidine ligands, as compared to those obtained with the cc-VTZ basis on the amidine ligands. Assuming that the same relationship between extrapolated values exists for model **2** Fe−CO BDEs,

TABLE 5: Mean Absolute Deviation of Iron−Imidazole, Iron−Ligand, and Average Iron−Porphyrin Nitrogen Bond Lengths Predicted by DFT, Relative to Crystal Structure Lengths

our model	crystal structure[a]	functional				
		BP86	BLYP	B3PW91	B3P86	B3LYP
^{5}FeP(Im)	myoglobin[68]	0.024	0.031	0.019	0.014	0.050
FeP(Im)(CO)	Fe(TPP)(CO)(1-MeIm)[66]	0.023	0.031	0.016	0.020	0.014
FeP(Im)(NO)	Fe(TPP)(NO)(1-MeIm)[67]	0.014	0.032	0.063	0.063	0.069
FeP(Im)(O$_2$)	Fe(TpivPP)(O$_2$)(2-MeIm)[63]	0.035	0.030	0.012	0.026	0.012
overall performance		0.024	0.031	0.027	0.031	0.036

[a] TPP = 5,10,15,20-tetraphenylporphyrin dianion. TpivPP = tetrakis(pivalamidophenyl)porphyrin.

the best estimate for the Fe−CO BDE for model **2** would be 12.0 kcal mol^{-1} instead of 13.0 kcal mol^{-1}. The B3LYP and B3PW91 values in Table 3 are extremely close to this value also. On the basis of this good agreement between B3LYP, B3PW91, and extrapolated CCSD(T) values of the Fe−CO bond energy for model **2**, we therefore expect that the predicted 18.1 and 18.0 kcal mol^{-1} Fe−CO bond energies for the larger FeP-(Im) model system should also be very accurate.

All functionals perform poorly in calculating the Fe−OH$_2$ BDE for model **1**. However, the CCSD(T) bond energy for this system is very negative, suggesting that it is not a very useful model for the full FeP(Im) system. In the case of model **2**, the pure functionals greatly overestimate the Fe−OH$_2$ BDE, but all the values predicted by the hybrid functionals are roughly acceptable. We observe that B3PW91, which is the closest match to our CCSD(T) energies, consistently predicts lower Fe-L BDEs (L = CO, H$_2$O, NO, and O$_2$, Tables 8−10) as compared to B3LYP. It is worth noting in this context that our B3LYP calculations on FeP(Im)(O$_2$) predict a positive bond energy, whereas B3PW91 predicts a negative bond energy. Since O$_2$ is known to bind to FeP(Im) even in the absence of supporting hydrogen bonds from a protein environment,[62] this suggests that B3LYP describes bonding to oxygen-containing ligands more accurately. This conflicting evidence means that we are unable to determine unequivocally whether the slightly weaker BDE predicted by B3PW91 as compared to the other two hybrid functionals is more accurate or not.

Our final calibration test for DFT is geometry prediction, and we find that all functionals perform well with respect to crystal structure geometries. Tables S2−S5 in the Supporting Information contain full details of optimized bond lengths and bond angles obtained with different DFT functionals for deoxy−FeP-(Im), FeP(Im)(CO), FeP(Im)(O$_2$), and FeP(Im)(NO), along with a full set of coordinates for our heme models. Not all of the experimental structures provide ideal reference points because the heme group may be distorted by the protein environment or by heme group side chains introduced so as to mimic the protein environment. For FeP(Im)(CO) and FeP(Im)(NO), we have been able to compare our geometries to crystal structures of similar unhindered heme groups and have included the protein or hindered model for comparison in the Supporting Information. For quintet deoxy−FeP(Im) and for FeP(Im)(O$_2$), such unhindered models are, to the best of our knowledge, unavailable, and our only reference points are either the protein or the hindered heme models that have been designed to mimic the protein,[63,64] both of which may distort the heme and ligand.

DFT functionals predict the Fe−L (L = CO, NO, and O$_2$) bond angles to a good level of accuracy. All the functionals predict Fe−C−O and Fe−N−O bond angles that differ by less than 2° from the equivalent unhindered models. Our Fe−O−O angles vary between 118.5 and 120.1° depending on the functional used. These values are smaller than those observed for highly hindered model compounds but are in good agreement

with the 122° angle in the oxy−myoglobin crystal structure[65] and the 118.1° found in another computational study.[38]

There are some systematic differences between bond lengths predicted by different functionals. For the pure functionals, the bond lengths predicted by BLYP are larger than those predicted by BP86. For the hybrid functionals, most of the bond lengths predicted by B3LYP are 0.01 to 0.03 Å larger than those predicted by B3PW91, and those predicted by B3PW91 are typically 0.01 Å higher than those predicted by B3P86. Some exceptions to this pattern are found in the bond lengths for FeP-(Im)(O$_2$), perhaps due to the use of the unrestricted method. For example, the Fe−O$_2$ bond length predicted by B3PW91 is longer than the B3LYP value, and the B3PW91 and B3P86 bond lengths are significantly more different from each other than found for the other compounds.

It is difficult to assess which functional is the most accurate because there are small discrepancies in bond lengths, even between similar models and between equivalent protein structures. Furthermore, for oxy− and deoxy−heme calibration, we can only compare our geometries against hindered models or crystal structures. It has been noted that the protein crystal structures are somewhat unreliable for metrics such as the Fe−L (L = CO, NO, and O$_2$) bond length due to the fitting procedure.[29,32] Table 5 shows the general accuracy of each functional in predicting bond lengths: this is indicated by calculating the mean absolute difference between the crystal structure and the calculated bond lengths for the iron−imidazole, iron−carbon, and average iron−porphyrin nitrogen bonds. For FeP(Im)(CO) and FeP(Im)(NO), the crystal structures used for comparison were the similar unhindered Fe(TPP)(CO)(1-MeIm)[66] and Fe(TPP)(NO)(1-MeIm)[67] models, where TPP is the 5,10,15,20-tetraphenylporphyrin dianion. For FeP(Im)(O$_2$) and deoxy-FeP(Im), the most similar structure was taken as the one with the lowest average bond length differences. For FeP-(Im)(O$_2$), this was the hindered Fe(TpivPP)(O$_2$)(2-MeIm) model,[63] where TpivPP is tetrakis(pivalamidophenyl)porphyrin, and for deoxy-FeP(Im), this was the high-resolution deoxy−myoglobin crystal structure of Kacholova et al.[68] The BP86 functional performs best overall, but the differences between different functionals, shown in Table 5, are not significant, especially considering the possible errors on the crystal structure and general DFT calculations. Overall, all of the DFT functionals assessed here predict reasonable geometries for heme-type compounds.

On the basis of this calibration work, we have explored the reactions of CO, H$_2$O, NO, and O$_2$ with the heme group using both the B3LYP functional used in our previous work[30] and the B3PW91 functional.

(2) Ligand Addition to the FeP(Im)−Heme Group. *Deoxy-heme System FeP(Im).* In our earlier B3LYP study of the reaction between CO and FeP(Im),[30] the quintet state of the latter fragment was found to be the ground state, with an energy 1.3 kcal mol^{-1} below the triplet. These calculations assumed

DFT Study of Ligand Binding to Heme

J. Phys. Chem. B, Vol. 111, No. 4, 2007 **847**

TABLE 6: Properties of the Deoxy−FeP(Im) Spin-States, Calculated with Restricted B3LYP[a]

species	E_{rel}[b]	d(Fe oop)[c]	r(Fe−N$_{Porp}$)[c]	jaw size[c]	r(Fe−N$_{Im}$)[c]
^{5}A′ deoxy	0.0 (0.0) [0.0 (0.0)]	−0.287 (−0.281)	2.095 (2.087)	2.075 (2.068)	2.214 (2.194)
^{3}A″ deoxy	−0.2 (2.8) [0.8 (3.5)]	−0.128 (−0.123)	2.022 (2.011)	2.018 (2.007)	2.306 (2.283)
^{1}S′ deoxy	5.1 (9.6) [7.7 (12.1)]	−0.142 (−0.131)	2.017 (2.003)	2.012 (1.999)	1.964 (1.936)

[a] Restricted B3PW91 values in parentheses. Energies calculated using the unrestricted ansatz with B3LYP and B3PW91 are shown between square brackets. [b] In kcal mol^{-1}. [c] In this table and subsequent ones, d(Fe oop) is the height of Fe above the xy-plane (defined as the plane of best fit through the four porphyrin nitrogens), r(Fe−N$_{Porp}$) is the average distance from Fe to the porphyrin nitrogens, the jaw size is half the average porphyrin cross-ring N−N distance, and r(Fe−N$_{Im}$) is the distance between Fe and the N atom of the coordinating imidazole; all distances are expressed in angstroms.

TABLE 7: Properties of FeP(Im)(CO) and FeP(Im)(OC) Calculated with Restricted B3LYP[a]

species	E_{rel}[b]	r(Fe−X)[c]	d(Fe oop)[c]	jaw size[c]	r(Fe−N$_{Im}$)[c]
^{1}A′-CO	−18.1 (−18.0)	1.806 (1.781)	+0.039 (+0.040)	2.028 (2.014)	2.075 (2.047)
^{1,3}MECP	+2.7 (+5.2)	2.542 (2.427)	−0.083 (−0.061)	2.027 (2.018)	2.193 (2.190)
^{1,5}MECP	+2.4 (+2.9)	2.323 (2.193)	−0.100 (−0.051)	2.080 (2.067)	2.220 (2.242)
^{3,5}MECP	+1.2 (+4.3)	3.105 (2.574)	−0.157 (−0.087)	2.053 (2.024)	2.309 (2.289)
^{1}A′-OC	+3.2 (+8.5)	2.282 (2.210)	+0.073 (+0.066)	2.019 (2.007)	1.982 (1.951)

[a] With restricted B3PW91 values in parentheses. [b] Relative to the sum of the CO ligand and the deoxy−FeP(Im) minimum (kcal mol^{-1}). [c] See footnote c in Table 6 for definitions of these distances.

that all states of FeP(Im) have a C_S symmetry, with the plane of symmetry including the iron atom, the imidazole proximal ligand, and two of the four porphyrin nitrogen atoms. We have since found that not all stationary points are minima with this symmetry and that rotation around the Fe−N(Im) bond leads to lower energies in some cases. The energy differences are small (1 kcal mol^{-1} or less, but together with the very slightly different basis set used here, account for the fact that we now find the B3LYP triplet FeP(Im) to lie below the quintet by 0.2 kcal mol^{-1} (Table 6). Another high-level DFT study[69] also found a triplet ground state with a close lying quintet state. Experimentally, deoxy−myoglobin is known to have a quintet ground state.[62] The calculated energy difference is small, and our calibration work suggests that B3LYP may overestimate the stability of the triplet, relative to the quintet, as already suggested elsewhere.[70] With B3PW91, the quintet state is found to be the ground state. It should in any case be noted that in myoglobin, the proximal histidine pulls the iron atom out of the heme plane, and this has been shown to stabilize the quintet relative to the triplet.[26,69]

The variation of our deoxy−FeP(Im) geometries with spin-state shows the generally expected trends for both the B3LYP and the B3PW91 functional. The B3PW91 functional systematically predicts slightly shorter bond lengths than the B3LYP functional, as seen in Supporting Information Tables S2−S5. The shorter Fe−N$_{Im}$ bond found by both functionals in the singlet state is expected due to the smaller d$_{z^2}$ orbital occupancy. The Fe out-of-plane (oop) distance and the heme core size or jaw size is greatest for the quintet spin-state, as is well-established.[71] Previous studies have shown that this is not because of the radius of the quintet iron(II), which is in fact smaller than the singlet or triplet.[37] We note that there is no correlation between the Fe oop distance and the Fe−N$_{Porp}$ bond length, jaw size, or Fe−N$_{Im}$ bond length.

Addition of CO to FeP(Im). The slight differences we find in the relative spin-state energies calculated by B3PW91 and B3LYP, reported here, have led us to revisit our previous characterization of the potential energy surfaces involved in the reaction of CO and FeP(Im).[30] Although we expect similar results for both functionals, based on the near-identical BDEs calculated by B3LYP and B3PW91 (18.1 and 18.0 kcal mol^{-1}, respectively), the higher energy predicted by B3PW91 for singlet FeP(Im) may cause a slightly higher energy barrier than previously reported for the spin-state change during CO

association/dissociation. We also wish to calculate the relative energy of FeP(Im)(OC), in which the CO ligand is bound to iron via oxygen, to check whether this may play a role in the binding of CO to deoxy−FeP(Im). The geometry of the MECPs and other points are summarized in Table 7.

Our CO bond energy of 18 kcal mol^{-1} is in good agreement with a computational value of 16.9 kcal mol^{-1} for a similar model.[38] The latter calculation included a continuum treatment of solvent effects, which should be small in the present case. It is in reasonable agreement with the Mb experimental[61] ΔH of binding of 10.8 kcal mol^{-1} once the correction for the zero-point energy of −4.4 kcal mol^{-1} is taken into account.[39] It is also possible (but by no means necessary, given the remaining uncertainties in the calculations) that the bond energy in the protein is slightly reduced due to steric effects,[39,72] which are of course absent in the model studied here. The relative energy of the FeP(Im)(OC) complex, with CO bound via the oxygen, is higher than the ^{1,5}MECP, so a singlet species of this type is unlikely to play a role in CO binding. In the unbound quintet state after photolysis in myoglobin, weak Fe−O interactions may occur.[73]

There are no FeP(Im)(CO) triplet or quintet states because the d$_{z^2}$ orbital on the iron of triplet or quintet deoxy−FeP(Im) is singly occupied, which prevents bonding interactions with the incoming CO ligand. Dispersion interactions will lead to shallow van der Waals minima, but dispersion is not well-described by DFT, so good results for such shallow minima cannot be expected. The report elsewhere of potential energy surfaces showing a quintet CO−FeP(Im) minimum is probably due to basis set superposition errors (BSSE).[31] The repulsive nature of the triplet and quintet surfaces leads to a spin-change induced barrier to recombination, for both the triplet to singlet process and the quintet to singlet one. The ^{1,5}MECP and ^{1,3}-MECP, calculated by B3LYP, lie 2.4 and 2.7 kcal mol^{-1}, respectively, above the energy of quintet deoxy−FeP(Im). Another computational study of the binding of CO to the heme group, in which approximately 1000 points were generated on the singlet and quintet PESs and then fitted to an analytical potential, finds no intrinsic barrier to the reaction but uses a substantially smaller basis set.[31] The B3PW91 functional calculates the ^{1,3}MECP and ^{3,5}MECP to be higher, presumably because it also predicts triplet and singlet deoxy−FeP(Im) to lie higher in energy relative to the quintet. The ^{1,5}MECPs calculated by both functionals are, however, similar in energy.

TABLE 8: Properties of FeP(Im)(OH₂), Calculated with Restricted B3LYP[a]

species	E_{rel}[b]	r(Fe–OH₂)[c]	d(Fe oop)[c]	jaw size[c]	r(Fe–N_Im)[c]
¹A′-OH₂	−12.7 (−8.1)	2.107 (2.087)	−0.061 (0.058)	2.024 (2.009)	2.008 (1.976)
¹,³MECP	−5.3 (−1.3)	2.343 (2.326)	−0.033 (−0.043)	2.024 (2.018)	2.250 (2.181)
¹,⁵MECP	−4.9 (−2.7)	2.281 (2.233)	−0.053 (−0.070)	2.067 (2.043)	2.212 (2.136)
³,⁵MECP	−5.1 (−2.0)	2.407 (2.470)	−0.028 (−0.018)	2.053 (2.026)	2.310 (2.238)
³A′-OH₂	−7.2 (−3.8)	3.224 (2.908)	−0.123 (−0.102)	2.019 (2.010)	2.313 (2.295)
⁵A′-OH₂	−7.8 (−7.4)	2.488 (2.474)	−0.139 (−0.143)	2.088 (2.080)	2.278 (2.250)

[a] With restricted B3PW91 values in parentheses. [b] Relative to the sum of the H₂O ligand and the deoxy–FeP(Im) minimum (kcal mol⁻¹). [c] See footnote c in Table 6 for definition of these distances
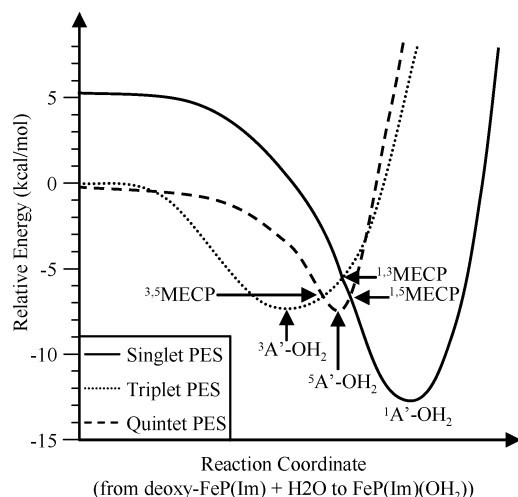

Figure 2. Schematic B3LYP potential energy surfaces for addition of H₂O to FeP(Im). The reaction coordinate roughly corresponds to the Fe–O distance.

Figure 3. Geometries of ³A′ FePIm(OH₂) (left), the ¹,⁵MECP between singlet and quintet potential energy surfaces (center), and the ¹A′ FePIm-(OH₂) bound form (right).

Both functionals thereby predict that the direct pathway leading from quintet deoxy–FeP(Im) to FeP(Im) –CO through a single MECP with a double spin-flip has a small but significant barrier of approximately 3 kcal mol⁻¹.

Addition of H₂O to FeP(Im). We next consider the reaction between H₂O and FeP(Im), which surprisingly, is predicted to be thermodynamically favorable (Table 8), although less so than the addition of CO. As discussed at the end of our BDE calibration work, the results in this paper suggest that the B3PW91 functional slightly underestimates the strength of Fe–O bonds. It is not, however, possible to tell with complete certainty whether the B3LYP BDE of 12.7 kcal mol⁻¹ or the B3PW91 BDE of 8.1 kcal mol⁻¹ is more accurate.

The singlet, triplet, and quintet PESs are all binding toward water (Figure 2), unlike for the analogous FeP(Im) reaction with CO where only the singlet PES is binding. Singlet PESs are binding toward both ligands because the d_{z^2} orbital, which points along the axis of the incoming sixth ligand, is empty and can participate in effective bonding with the incoming ligand. In the triplet and quintet states of deoxy–heme, there is one electron in the d_{z^2} orbital. This means that orbital-based σ-bonding interactions lead to three-electron two-center bonding, which is probably mostly repulsive and dominant for the nonpolar CO ligand. As H₂O binds along the triplet and quintet surfaces, this repulsive interaction is more than compensated for by the larger stabilizing electrostatic attraction between the water dipole and the partial positive charge on the iron. The triplet and quintet surfaces are, however, more weakly bound than the singlet.

As was the case for CO binding to deoxy–FeP(Im), there is no direct correlation between the Fe–OH₂ bond length, Fe oop distance, the heme jaw size, and the Fe–N_Im bond length. As H₂O binds to deoxy–FeP(Im), the longer Fe–OH₂ distance
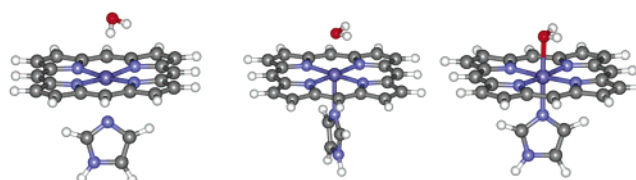
(Table 8) indicates that the triplet minimum is situated earlier along the reaction coordinate than the quintet minimum. In fact, the triplet does not really involve an Fe–O bond, with the H₂O ligand instead donating two hydrogen bonds to the nitrogen atoms of the porphyrin ring (Figure 3). The geometries of the three surface crossing points located here, ¹,³MECP, ³,⁵MECP, and ¹,⁵MECP, are fairly similar to one another and involve a more marked Fe–O interaction. The most strongly bound species in terms of energy, the singlet FeP(Im)(OH₂) complex, also has the shortest Fe–O distance.

The three MECPs between singlet, triplet, and quintet surfaces (Figure 3 and Table 8) occur 4.9−5.3 kcal mol⁻¹ below the energy of the separated quintet deoxy–FeP(Im) and H₂O fragments, so there is no energy barrier associated with the addition of H₂O to the heme group. The direct pathway for the association of H₂O to deoxy–FeP(Im) involves either conversion through ³,⁵MECP to the triplet adduct followed by a second spin-flip or by a direct double spin-flip at ¹,⁵MECP. The energies of the triplet and quintet local minima and crossing points are very similar when calculated with the B3LYP functional, but the triplet surface is found to be less stable than the quintet surface with the B3PW91 functional, as was found for deoxy–FeP(Im) relative spin-states in our calibration studies. The local minima described here may explain the tunneling of water, observed experimentally for the reaction with ferrous deoxy–myoglobin below 50 K,[74] as this tunneling could occur through the barrier between the quintet and the singlet FeP(Im)(OH₂) complex. However, the PESs of the water binding reaction do not explain the experimental observation that H₂O only binds to myoglobin under specific circumstances. We suggest that in the protein environment, the water molecule is stabilized by hydrogen bonding within the distal pocket, which prevents bond formation. The bonded adduct may also be destabilized by small steric and strain effects, as found for CO binding.[39] Taken together, these influences may make water binding thermodynamically unfavorable in the protein's deoxy tertiary structure.

Addition of NO to FeP(Im). This process is known to be thermodynamically favorable in myoglobin,[75] which is verified by our B3LYP calculated BDE of 12.7 kcal mol⁻¹, in excellent agreement with another computational study of a similar model.[38] Experimentally, the equilibrium constant for NO binding to the heme center in myoglobin is large,[75] larger than those for CO or O₂ binding. Analysis of the experimental data[38] suggests a binding enthalpy of ca. 20 kcal mol⁻¹. As also noted

DFT Study of Ligand Binding to Heme

J. Phys. Chem. B, Vol. 111, No. 4, 2007 **849**

in that paper,[38] if this experimental value is correct, then typical B3LYP calculated Fe−NO BDEs, such as our value of 12.7 kcal mol^{-1}, are somewhat too weak. Hydrogen bonding in myoglobin between the bound ligand and a histidine residue located above the heme group (the distal histidine) plays an important role in stabilizing bound dioxygen but is not expected to significantly strengthen bonding to NO.[29,38] Indeed, mutation of the distal histidine to an apolar amino acid barely changes the equilibrium constant for NO binding, corresponding to a change in binding energy of at most 1 kcal mol^{-1}.[75]

We have calculated the bond energy of NO to the ground state, triplet, iron porphine (that is, the present deoxy−heme model, but without the imidazole ligand), using the B3LYP functional and the same basis sets as for the other calculations. The resulting value of 7.3 kcal mol^{-1} means that there is a small decrease in BDE as a result of removing the imidazole, as observed in a previous computational study.[28] Experimental binding enthalpies of ca. 25 kcal mol^{-1} have been reported for NO binding to various cationic iron−porphine species in the gas phase.[76] Many of these species contain an iron(III) center so are not directly comparable to the results obtained here. However, one compound, a monoprotonated derivative of tetrapyridinylporphine, contains Fe(II) and has a bond energy of 26.6 kcal mol^{-1}. This suggests that the present B3LYP calculated bond energies for NO are too small. Previous work using non-hybrid functionals[28] gives much larger bond energies, so the trends found for CO and H_2O binding in our calibration work, whereby B3LYP gives accurate bond energies, may not be applicable to NO binding. However, computational restrictions mean that we have not been able to carry out CCSD(T) calibration calculations for NO binding.

We find that the quartet and sextet PESs involved in the association of NO with deoxy−FeP(Im) are weakly binding toward NO. In the case of the sextet state, in which there is no bonding interaction between doublet NO and quintet deoxyheme fragments, this suggests that electrostatic stabilization from interactions between the NO nitrogen and the heme iron compensate for the weakly repulsive orbital interactions, although not as strongly as for H_2O binding given the lower polarity of NO. Although a quartet state with Fe−N covalent bonding is formally possible, we find instead that the lowest-lying quartet is a weak adduct between a triplet deoxyheme fragment and NO, as shown by the heme geometry, which is similar to that of triplet FeP(Im), and the electronic structure, with two unpaired electrons on Fe and one on NO. This also accounts for the low bond energy. The doublet, as discussed previously, is more strongly bound and includes significant Fe−N covalent bonding. The unpaired electron is situated mainly on NO, as found elsewhere.[38]

Experimentally, the reaction of NO and Mb occurs extremely readily, even more so than that of CO and Mb.[6,10] Flash photolysis experiments and molecular dynamics simulations indicate that there is a small barrier to NO rebinding but that this barrier increases as myoglobin undergoes conformational relaxation.[8,9,17,77] Our calculated PESs and surface crossings show that there is a small intrinsic energy barrier to addition (Figure 4). Starting on the sextet surface, there is one low-energy pathway through ^{4,6}MECP and ^{2,4}MECP with a maximum energy (at ^{4,6}MECP) of 0.8 kcal mol^{-1} relative to the quintet fragments. Because quintet deoxyheme and NO correlate without a spin-state change with the quartet adduct, there is also a lower energy pathway leading directly to the quartet adduct then crossing ^{2,4}MECP, which lies 0.2 kcal mol^{-1} lower than the quintet deoxyheme and NO fragments (and 1.6 kcal
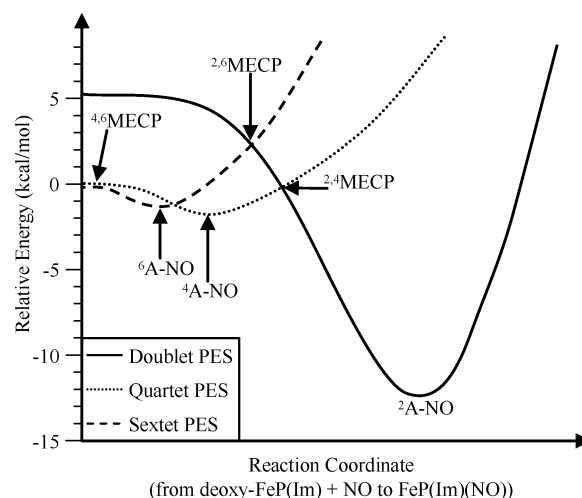

Figure 4. Schematic B3LYP potential energy surfaces for addition of NO to FeP(Im). The reaction coordinate roughly corresponds to the Fe−N distance.

TABLE 9: Properties of FeP(Im)(NO), FeP(Im)(ON), and Deoxy−FeP(Im), Calculated with Restricted Open-Shell B3LYP

species	E_{rel}[a]	r(Fe−X)[b]	d(Fe oop)[b]	jaw size[b]	r(Fe−N$_{Im}$)[b]
^{2}A-NO	−12.7 (−10.6)	1.811	+0.030	2.026	2.060
^{2}A-ON	+0.3 (+5.1)	2.100	−0.049	2.021	1.993
^{4}A-NO	−1.8	2.934	−0.106	2.019	2.315
^{6}A-NO	−1.6	3.503	−0.275	2.077	2.209
^{2,4}MECP	−0.2	2.302	−0.035	2.022	2.211
^{2,6}MECP	+2.5	2.366	−0.075	2.070	2.154
^{4,6}MECP	+0.8	3.521	−0.209	2.047	2.264

[a] Relative to the sum of the NO ligand and the quintet deoxy−FeP(Im) minimum (kcal mol^{-1}). B3PW91 energy in parentheses. [b] See footnote c of Table 6 for definitions of these distances.

TABLE 10: Properties of Ground State FeP(Im)(O₂), Calculated with Unrestricted Open-Shell B3LYP[a]

species	E_{rel}[b]	r(Fe−O)[c]	d(Fe oop)[c]	jaw size[c]	r(Fe−N$_{Im}$)[c]
^{1}Fe−O$_2$	−2.83 (+2.06)	1.899	+0.017	2.020	2.119

[a] With the B3PW91 energy in parentheses. [b] Relative to the sum of the NO ligand and the quintet deoxy−FeP(Im) minimum (kcal mol^{-1}). [c] See footnote c in Table 6 for definitions of these distances.

mol^{-1} above the quartet minimum). As well as involving a lower barrier than CO rebinding, the key step here only involves a change in spin of one electron, instead of two for CO rebinding, and these two factors presumably explain the faster rebinding.

Because the important surface crossings occur well before the doublet NO minimum, the fact that the enthalpy of the latter species is apparently not well-reproduced using hybrid DFT may not affect our results concerning the barrier heights too significantly. If anything, the key ^{2,4}MECP will be lower in energy than calculated here.

We have also explored two hypotheses about NO binding to the heme group. First, an alternative pathway to NO binding has been proposed by Nutt et al., via a local minimum they located on the doublet [FeP(Im),(NO)] potential energy surface corresponding to a metastable FeP(Im)(ON) complex, which they suggest may isomerize to FeP(Im)(NO).[15] With the larger basis set used in this study, we find that this FeP(Im)(ON) species is higher in energy than the sum of the NO ligand and the quintet deoxy−FeP(Im) fragment (Table 9). Therefore, we do not expect this species to be involved during NO binding to FeP(Im)(NO), and it does not explain the differences in NO and CO binding in myoglobin by providing an alternative lower energy pathway.

The second hypothesis is a so-called harpoon mechanism,[14] whereby the Fe—NO bond can form without the heme iron having to move into the porphyrin plane, unlike CO and H_2O binding. CO and O_2 require concerted motion of the protein and the heme group and so do not bind as readily. Our model does not support this harpoon mechanism because we do not see a strong (i.e., short) Fe—N bond until the heme iron has moved into the plane, in the ^{2}FeP(Im)(NO) adduct. The faster geminate rebinding observed for photolyzed nitrosyl—myoglobin as compared to carbonmonoxy—myoglobin is clearly due to the smaller spin-change induced barrier for NO as compared to CO. The difference between NO and O_2 binding is less clear because there is likely to be no significant intrinsic barrier for O_2 binding. The different behavior may be due to dynamical features within the protein.

Addition of O_2 to FeP(Im). We will treat this only briefly as the PESs associated with the binding of O_2 with deoxy—FeP-(Im) have been previously characterized by Jensen et al.,[36] who used DFT to optimize symmetry restricted FeP(Im)(O_2) molecules with fixed and systematically increasing Fe—O bond lengths. They found that at least one spin-state change is required for the binding of O_2 to the heme group and that this spin-state change occurs easily due to a broad crossing region of five electronic states of similar low energy as O_2 begins to bind. This mirrors our observations for NO stated previously, and we expect that the relevant MECPs would lie at low energy, although they were not explicitly located.[36] In another study, O_2 binding to the heme group is predicted to involve a significant barrier, but this work did not allow for heme group relaxation toward changes in the Fe—O distance and hence does not realistically reproduce the PESs of this reaction.[34] As we do not expect the crossing behavior to differ significantly from that found by Jensen et al., we have not located MECPs for this system but, for completeness, have calculated the bond energy for the singlet ground state of FeP(Im)(O_2). In this case, we have used unrestricted B3LYP to describe the open-shell singlet character of this state,

The ground state of FeP(Im)(O_2) is known to be a singlet from electron paramagnetic resonance experiments.[62] Our calculations lead to an electronic state that is an open-shell singlet with spin-polarization over the Fe—O bond,[26,29,78] which suggests a large component of the ^{2}Fe^{3+}—^{2}O$_2^-$ Weiss model configuration.[79] Blomberg et al. calculate a binding enthalpy of 7.6 kcal mol^{-1} for their heme model.[38] This includes a 2.5 kcal mol^{-1} correction for the fact that the open-shell singlet state is in fact a mixture of singlet and triplet states, which we have not included. Our study also uses a different basis set, an imidazole axial ligand instead of NH_3, and is carried out on an isolated molecule instead of using a continuum solvent model. Taking these differences into account, the two results are very similar.

Conclusion

In this paper, DFT and ab initio correlated CCSD(T) calculations were used to characterize the potential energy surfaces for binding of CO, H_2O, NO, and O_2 to models of the heme group. A first set of calculations focuses on two small models of the heme group. For these systems, DFT as well as accurate large basis set CCSD(T) calculations are feasible, enabling calibration of the former methods. We estimate that the CCSD(T) relative spin-state energetics and bond energies for the small models are accurate to within 5 kcal mol^{-1} and probably better. Our calculations show that the gradient corrected functionals BLYP and BP86 do not describe the energetics of these systems accurately. In contrast, the hybrid functionals, especially B3PW91 and B3LYP and especially for the more realistic model **2**, are in very good agreement with CCSD(T). We have also compared optimized geometries for a larger model of the heme group with experimental structures and find that all the functionals yield reasonable results.

On the basis of these results, we have used the B3LYP and B3PW91 functionals to explore the potential energy surfaces for binding of four small ligands, CO, H_2O, NO, and O_2, to the heme group. The use of a modest-sized, isolated model means that our calculations probe the intrinsic electronic barriers to binding. Experimental behavior in proteins such as myoglobin results from a combination of these intrinsic electronic effects as well as the steric and electronic effects of the protein environment. Although previous DFT studies have already explored the binding energy of some of the ligands, for consistency, we report calculated bond energies for all the ligands. Except for H_2O, which has not been studied before, our calculations are in good agreement with previous work. For CO and O_2, our calculated bond energies are also fairly close to the experimentally derived values. It should be noted that different experimental approaches sometimes lead to significantly different values, so caution is required when comparing with experiment. For NO, our calculated bond energy is smaller than the experimental value, and this may be due to a less accurate performance of B3LYP for this system.

Binding of CO to deoxyheme is found to involve a significant barrier of ca. 3 kcal mol^{-1}, due to the need to cross from the quintet potential energy surface to the singlet state. This barrier explains the relatively slow geminate recombination of CO upon photolysis of carbonmonoxy—myoglobin.

Water does not usually bind to the ferrous iron of deoxy—myoglobin, but under special conditions, a bound water complex can be formed, and geminate recombination is observed upon laser photolysis of the Fe—OH$_2$ bond.[13,74] Our calculations show that water can bind to the heme group to form a weakly bound singlet state. We also find that the need to change spin-state from quintet deoxy—heme to the singlet bound state does not lead to a large barrier to addition; indeed, the MECPs between quintet, triplet, and singlet states lie lower in energy than the separated fragments. These results suggest that the observed lack of binding in proteins such as myoglobin is not due to a very weak intrinsic bond energy, or to the existence of a large barrier, but to a decrease in the bond energy for water in the presence of the protein environment. This modulation of the iron—water bond energy is in fact dependent on the detailed tertiary structure of the protein, as under special conditions, water will actually bind to the heme group, in agreement with our calculated intrinsic potential energy surface.

For binding of NO, we have found that the need to change the spin-state only creates a very small barrier. Depending on whether binding starts on the sextet or quartet potential energy surface, this barrier lies 0.8 kcal mol^{-1} above or 0.2 kcal mol^{-1} below the separated fragments. This is consistent with the observed rapid binding of NO. The fact that B3LYP underestimates the bond energy for NO should not affect this conclusion. A previous suggestion that NO binds more rapidly than CO to the heme group due to the possibility of forming an intermediate oxygen bound adduct can be discounted, as this Fe—ON isomer is found to lie higher in energy than the separated fragments upon using a large basis set. Finally, for binding of O_2, we have not located the MECPs, but these are expected to lie fairly low in energy, based on a previous DFT study.

DFT Study of Ligand Binding to Heme

J. Phys. Chem. B, Vol. 111, No. 4, 2007 **851**

Supporting Information Available: CCSD energies (kcal mol^{-1}, relative to the quintet state) of triplet and singlet states of model heme compounds and key structural features of FeP-(Im)(X) geometries, calculated with different functionals and a full set of coordinates of heme groups and models. This material is available via the Internet at http://pubs.acs.org.

References and Notes

(1) Richter-Addo, G. B.; Legzdins, P.; Burstyn, J. *Chem. Rev.* **2002**, *102*, 857.

(2) Beltran, B.; Quintero, M.; Garcia-Zaragoza, E.; O'Connor, E.; Esplugues, J. V.; Moncada, S. *Proc. Natl. Acad. Sci. U.S.A.* **2002**, *99*, 8892.

(3) (a) Garthwaite, J. *Trends Neurosci.* **1991**, *14*, 60. (b) Dawson, T.; Dawson, D.; Synder, S. *Ann. Neurol.* **1992**, *32*, 297.

(4) Austin, R. H.; Beeson, K. W.; Eisenstein, L.; Frauenfelder, H.; Gunsalus, I. C. *Biochemistry* **1975**, *14*, 5355.

(5) Cornelius, P. A.; Hochstrasser, R. M.; Steele, A. W. *J. Mol. Biol.* **1983**, *163*, 119.

(6) Petrich, J. W.; Lambry, J. C.; Kuczera, K.; Karplus, M.; Poyart, C.; Martin, J. L. *Biochemistry* **1991**, *30*, 3975.

(7) (a) Steinbach, P. J.; Ansari, A.; Berendzen, J.; Braunstein, D.; Chu, K.; Cowen, B. R.; Ehrenstein, D.; Frauenfelder, H.; Johnson, J. B.; Lamb, D. C.; Luck, S.; Mourant, J. R.; Nienhaus, G. U.; Ormos, P.; Philipp, R.; Xie, A. H.; Young, R. D. *Biochemistry* **1991**, *30*, 3988. (b) Ye, X.; Demidov, A.; Champion, P. M. *J. Am. Chem. Soc.* **2002**, *124*, 5914.

(8) Petrich, J. W.; Lambry, J. C.; Balasubramanian, S.; Lambright, D. G.; Boxer, S. G.; Martin, J. L. *J. Mol. Biol.* **1994**, *238*, 437.

(9) Walda, K. N.; Liu, X. Y.; Sharma, V. S.; Magde, D. *Biochemistry* **1994**, *33*, 2198.

(10) Olson, J. S.; Phillips, G. N. *J. Biol. Chem.* **1996**, *271*, 17593.

(11) Alberding, N.; Austin, R. H.; Beeson, K. W.; Chan, S. S.; Eisenstein, L.; Frauenfelder, H.; Nordlund, T. M. *Science* **1976**, *192*, 1002.

(12) Lamb, D. C.; Ostermann, A.; Prusakov, V. E.; Parak, F. G. *Eur. Biophys. J. Biophys. Lett.* **1998**, *27*, 113.

(13) Lamb, D. C.; Prusakov, V.; Engler, N.; Ostermann, A.; Schellenberg, P.; Parak, F. G.; Nienhaus, G. U. *J. Am. Chem. Soc.* **1998**, *120*, 2981.

(14) Ionascu, D.; Gruia, F.; Ye, X.; Yu, A. C.; Rosca, F.; Beck, C.; Demidov, A.; Olson, J. S.; Champion, P. M. *J. Am. Chem. Soc.* **2005**, *127*, 16921.

(15) Nutt, D. R.; Karplus, M.; Meuwly, M. *J. Phys. Chem. B* **2005**, *109*, 21118.

(16) Greene, B. I.; Hochstrasser, R. M.; Weisman, R. B.; Eaton, W. A. *Proc. Natl. Acad. Sci. U.S.A.* **1978**, *75*, 5255.

(17) Petrich, J. W.; Poyart, C.; Martin, J. L. *Biochemistry* **1988**, *27*, 4049.

(18) Harvey, J. N.; Poli, R.; Smith, K. M. *Coord. Chem. Rev.* **2003**, *238*, 347.

(19) Poli, R.; Harvey, J. N. *Chem. Soc. Rev.* **2003**, *32*, 1.

(20) Smith, K. M.; Poli, R.; Harvey, J. N. *New J. Chem.* **2000**, *24*, 77.

(21) (a) Smith, K. M.; Poli, R.; Harvey, J. N. *Chem.—Eur. J.* **2001**, *7*, 1679. (b) Harvey, J. N.; Aschi, M. *Faraday Discuss.* **2003**, *124*, 129.

(22) (A) Green, J. C.; Harvey, J. N.; Poli, R. *J. Chem. Soc., Dalton Trans.* **2002**, 1861. (b) Harvey, J. N.; Poli, R. *Dalton Trans.* **2003**, 4100.

(23) Carreón-Macedo, J.-L.; Harvey, J. N. *J. Am. Chem. Soc.* **2004**, *126*, 5789.

(24) (a) Bytheway, I.; Hall, M. B. *Chem. Rev.* **1994**, *94*, 639. (b) Vogel, K. M.; Kozlowski, P. M.; Zgierski, M. Z.; Spiro, T. G. *J. Am. Chem. Soc.* **1999**, *121*, 9915. (c) Marechal, J. D.; Barea, G.; Maseras, F.; Lledos, A.; Mouawad, L.; Perahia, D. *J. Comput. Chem.* **2000**, *21*, 282. (d) Rovira, C.; Parrinello, M. *Biophys. J.* **2000**, *78*, 93. (e) Spiro, T. G.; Zgierski, M. Z.; Kozlowski, P. M. *Coord. Chem. Rev.* **2001**, *219*, 923. (f) Zhang, Y.; Gossman, W.; Oldfield, E. *J. Am. Chem. Soc.* **2003**, *125*, 16387. (g) Rydberg, P.; Sigfridsson, E.; Ryde, U. *J. Biol. Inorg. Chem.* **2004**, *9*, 203.

(25) (a) Jewsbury, P.; Yamamoto, S.; Minato, T.; Saito, M.; Kitagawa, T. *J. Phys. Chem.* **1995**, *99*, 12677. (b) Menyhard, D. K.; Keseru, G. M. *J. Am. Chem. Soc.* **1998**, *120*, 7991. (c) Rovira, C.; Parrinello, M. *Chem.—Eur. J.* **1999**, *5*, 250. (d) De Angelis, F.; Jarzecki, A. A.; Car, R.; Spiro, T. G. *J. Phys. Chem. B* **2005**, *109*, 3065.

(26) Rovira, C.; Kunc, K.; Hutter, J.; Ballone, P.; Parrinello, M. *J. Phys. Chem. A* **1997**, *101*, 8914.

(27) Maseras, F. *New J. Chem.* **1998**, *22*, 327.

(28) Rovira, C.; Kunc, K.; Hutter, J.; Ballone, P.; Parrinello, M. *Int. J. Quantum Chem.* **1998**, *69*, 31.

(29) Sigfridsson, E.; Ryde, U. *J. Biol. Inorg. Chem.* **1999**, *4*, 99.

(30) Harvey, J. N. *J. Am. Chem. Soc.* **2000**, *122*, 12401.

(31) McMahon, B. H.; Stojkovic, B. P.; Hay, P. J.; Martin, R. L.; Garcia, A. E. *J. Chem. Phys.* **2000**, *113*, 6831.

(32) (a) Rovira, C.; Schulze, B.; Eichinger, M.; Evanseck, J. D.; Parrinello, M. *Biophys. J.* **2001**, *81*, 435. (b) Sigfridsson, E.; Ryde, U. *J. Inorg. Biochem.* **2002**, *91*, 101.

(33) Franzen, S. *J. Phys. Chem. B* **2002**, *106*, 4533.

(34) Franzen, S. *Proc. Natl. Acad. Sci. U.S.A.* **2002**, *99*, 16754.

(35) Scherlis, D. A.; Estrin, D. A. *Int. J. Quantum Chem.* **2002**, *87*, 158.

(36) Jensen, K. P.; Ryde, U. *J. Biol. Chem.* **2004**, *279*, 14561.

(37) Ugalde, J. M.; Dunietz, B.; Dreuw, A.; Head-Gordon, M.; Boyd, R. J. *J. Phys. Chem. A* **2004**, *108*, 4653.

(38) Blomberg, L. M.; Blomberg, M. R. A.; Siegbahn, P. E. M. *J. Inorg. Biochem.* **2005**, *99*, 949.

(39) Strickland, N.; Mulholland, A. J.; Harvey, J. N. *Biophys. J.* **2006**, *90*, L27–L29.

(40) Harvey, J. N. *Faraday Discuss.* **2004**, *127*, 165.

(41) Becke, A. D. *J. Chem. Phys.* **1993**, *98*, 5648.

(42) Curtiss, L. A.; Raghavachari, K.; Redfern, P. C.; Pople, J. A. *J. Chem. Phys.* **1997**, *106*, 1063.

(43) Siegbahn, P. E. M.; Blomberg, M. R. A. *Annu. Rev. Phys. Chem.* **1999**, *50*, 221.

(44) Siegbahn, P. E. M.; Blomberg, M. R. A. *Chem. Rev.* **2000**, *100*, 421.

(45) (a) Reiher, M.; Salomon, O.; Hess, B. A. *Theor. Chem. Acc.* **2001**, *107*, 48. (b) Salomon, O.; Reiher, M.; Hess, B. A. *J. Chem. Phys.* **2002**, *117*, 4729. (c) Harvey, J. N. *Struct. Bonding (Berlin)* **2004**, *112*, 151.

(46) Perdew, J. D. *Phys. Rev. B* **1986**, *33*, 8822.

(47) Becke, A. D. *Phys. Rev. A* **1988**, *38*, 3098.

(48) (a) Choe, Y. K.; Nakajima, T.; Hirao, K.; Lindh, R. *J. Chem. Phys.* **1999**, *111*, 3837. (b) Ghosh, A.; Taylor, P. R. *Curr. Opin. Chem. Biol.* **2003**, *7*, 113. (c) Ghosh, A.; Persson, B. J.; Taylor, P. R. *J. Biol. Inorg. Chem.* **2003**, *8*, 507. (d) Pierloot, K. *Mol. Phys.* **2003**, *101*, 2083.

(49) Newton, J. E.; Hall, M. B. *Inorg. Chem.* **1984**, *23*, 4627.

(50) *Jaguar 6.0*; Schrodinger, LLC: Portland, OR, 2005.

(51) Lee, C. T.; Yang, W. T.; Parr, R. G. *Phys. Rev. B* **1988**, *37*, 785.

(52) Perdew, J. P.; Chevary, J. A.; Vosko, S. H.; Jackson, K. A.; Pederson, M. R.; Singh, D. J.; Fiolhais, C. *Phys. Rev. B* **1992**, *46*, 6671.

(53) Edgecombe, K. E.; Becke, A. D. *Chem. Phys. Lett.* **1995**, *244*, 427.

(54) *MOLPRO*; A package of ab inito programs designed by H.-J. Werner and P. J. Knowles with contributions from R. D. Amos, A. Bernhardsson, A. Berning, P. Celani, D. L. Cooper, M. J. O. Deegan, A. J. Dobbyn, F. Eckert, C. Harmpel, G. Hetzer, P. J. Knowles, T. Korona, R. Lindh, A. W. Lloyd, S. J. McNicholas, F. R. Manby, W. Meyer, M. E. Mura, A. Nicklass, P. Palmieri, R. Pitzer, G. Rauhut, M. Schutz, U. Schumann, H. Stoll, A. J. Stone, R. Tarroni, T. Thorsteinsson, and H.-J. Werner University of Birmingham: Birmingham, UK, 2002.

(55) Dunning, T. H. *J. Chem. Phys.* **1989**, *90*, 1007.

(56) Ricca, A.; Bauschlicher, C. W. *Theor. Chem. Acc.* **2001**, *106*, 314.

(57) Helgaker, T.; Klopper, W.; Koch, H.; Noga, J. *J. Chem. Phys.* **1997**, *106*, 9639.

(58) Harvey, J. N.; Aschi, M.; Schwarz, H.; Koch, W. *Theor. Chem. Acc.* **1998**, *99*, 95.

(59) Watts, J. D.; Urban, M.; Bartlett, R. J. *Theor. Chim. Acta* **1995**, *90*, 341.

(60) Lee, T. J.; Taylor, P. R. *Int. J. Quantum Chem., Quantum Chem. Symp.* **1989**, *23*, 199.

(61) Projahn, H. D.; Van Eldik, R. *Inorg. Chem.* **1991**, *30*, 3288.

(62) Momenteau, M.; Reed, C. A. *Chem. Rev.* **1994**, *94*, 659.

(63) Jameson, G. B.; Rodley, G. A.; Robinson, W. T.; Gagne, R. R.; Reed, C. A.; Collman, J. P. *Inorg. Chem.* **1978**, *17*, 850.

(64) Jameson, G. B.; Molinaro, F. S.; Ibers, J. A.; Collman, J. P.; Brauman, J. I.; Rose, E.; Suslick, K. S. *J. Am. Chem. Soc.* **1980**, *102*, 3224.

(65) Vojtechovsky, J.; Chu, K.; Berendzen, J.; Sweet, R. M.; Schlichting, I. *Biophys. J.* **1999**, *77*, 2153.

(66) Peng, S. M.; Ibers, J. A. *J. Am. Chem. Soc.* **1976**, *98*, 8032.

(67) Scheidt, W. R.; Piciulo, P. L. *J. Am. Chem. Soc.* **1976**, *98*, 1913.

(68) Kachalova, G. S.; Popov, A. N.; Bartunik, H. D. *Science* **1999**, *284*, 473.

(69) Kozlowski, P. M.; Spiro, T. G.; Zgierski, M. Z. *J. Phys. Chem. B* **2000**, *104*, 10659.

(70) Liao, M. S.; Scheiner, S. *J. Chem. Phys.* **2002**, *116*, 3635.

(71) Perutz, M. F. *Nature* **1970**, *228*, 726.

(72) Springer, B. A.; Sligar, S. G.; Olson, J. S.; Phillips, G. N. *Chem. Rev.* **1994**, *94*, 699.

(73) (a) Vitkup, D.; Petsko, G. A.; Karplus, M. *Nat. Struct. Biol.* **1997**, *4*, 202. (b) Nutt, D. R.; Meuwly, M. *Biophys. J.* **2003**, *85*, 3612. (c) Nutt, D. R.; Meuwly, M. *Proc. Natl. Acad. Sci. U.S.A.* **2004**, *101*, 5998.

(74) Lamb, D. C.; Kriegl, J.; Kastens, K.; Nienhaus, G. U. *J. Phys. Org. Chem.* **2000**, *13*, 659.

(75) Olson, J. S.; Phillips, G. N. *J. Biol. Inorg. Chem.* **1997**, *2*, 544.

(76) Chen, O. N.; Groh, S.; Liechty, A.; Ridge, D. P. *J. Am. Chem. Soc.* **1999**, *121*, 11910.

(77) (a) Meuwly, M.; Becker, O. M.; Stote, R.; Karplus, M. *Biophys. Chem.* **2002**, *98*, 183. (b) Kim, S.; Jin, G.; Lim, M. *J. Phys. Chem. B* **2004**, *108*, 20366. (c) Meuwly, M.; Nutt, D. R. *Biophys. J.* **2006**, *90*, 1191.

(78) (a) Kaupp, M.; Rovira, C.; Parrinello, M. *J. Phys. Chem. B* **2000**, *104*, 5200. (b) Jensen, K. P.; Roos, B. O.; Ryde, U. *J. Inorg. Biochem.* **2005**, *99*, 978.

(79) (a) Weiss, J. J. *Nature* **1964**, *202*, 83. (b) Goddard, W. A.; Olafson, B. D. *Proc. Natl. Acad. Sci. U.S.A.* **1975**, *72*, 2335.